International Forum on Aeroelasticity and Structural Dynamics
IFASD 2019
9-13 June 2019, Savannah, Georgia, USA

FLUTTER SENSITIVITY ANALYSIS FOR WING PLANFORM OPTIMIZATION

Francesco Torrigiani[1], Jan-Niclas Walther[1], Rocco Bombardieri[2], Rauno Cavallaro[2], Pier Davide Ciampa[1]

[1]DLR, German Aerospace Center,
Institute of System Architectures in Aeronautics
Hamburg, Germany
francesco.torrigiani@dlr.de

[2]University Carlos III of Madrid
Leganes, Madrid, Spain
rauno.cavallaro@uc3m.es

Keywords: unsteady aerodynamic differentiation, modal shapes derivative, Morino's method.

Abstract: The increased airframe flexibility of the new generation of commercial aircrafts, and the unreliability, for unconventional aircraft configurations, of the classical statistical-based aeroelastic methods, require the introduction of physics-based aeroelastic analysis in the early development stages of the overall aircraft synthesis process. The paper presents a differentiated unsteady aeroelastic analysis module suitable for the large scale MDO problem typical of preliminary aircraft design. Morino's method is implemented and deployed for the frequency domain aerodynamic analysis. This method is able to deal with arbitrary complex 3D body surfaces increasing the geometrical fidelity and the robustness of the analysis procedure. Finite state aerodynamic modeling is adopted to represent the aerodynamic term in the aeroelastic equation allowing the use of simple root locus method for the flutter point definition. The interface with the central data model, CPACS, allows the deployment of the aeroelastic module in collaborative multi-disciplinary design workflows. The total derivative of flutter speed is computed analytically, whereas for some partial derivatives complex step approach resulted more convenient. Since derivatives with respect to wing planform parameters, such us span and sweep angle, are sought, the derivatives of the structural modal shapes cannot be neglected and are analytically computed. For the total derivative of the aerodynamic term in the aeroelastic equation, the GAF matrix, we developed a discrete adjoint method. Finally, the Goland's wing benchmark case is used for flutter analysis validation, and, for this configuration, derivatives with respect to span and sweep angle are computed and compared with finite difference results.

1 INTRODUCTION

In the conceptual and preliminary development phases, flexibility effects are conventionally not included in the design investigations. At best, aeroelastic instabilities are estimated by empirical relations and available data from previous designs, rather than by incorporating physics-based analyses. Hence, at these stages the estimation of the relevant load cases includes conservative allowances and safety margins for the structural design in order to guarantee the structural integrity. This rather conventional sequential design approach usually adds an "aeroelastic

penalty" to the final designed structure [1]. However, with the increasing efficiency of the structural design concepts, the importance of flexibility is significantly growing: its effects need to be properly accounted from the beginning of the development in order to minimize expensive redesign activities or the degradation of the prospected performance.
As Ref. [2] pointed out, although well-established methods are available for linear aeroelastic analyses of modern airplanes, there is still a limited capacity to bring them into the early stages of the design process. Steady high-fidelity aeroelastic analysis has been already successful integrated in a multidisciplinary design process. The obtained optimal wings show a significant increase of the aerodynamic efficiency, up to 20%, but the excessively high aspect ratio suggests possible flutter instability [3, 4]. When flutter constraints are included in the overall aircraft design process (OAD), they highly affect the optimal solution, as shown by Ref. [5]. For instance, flutter-free configurations show a higher structural mass and a lower aspect ratio wing. The same trend have been also observed for unconventional configurations.

In order to further foster the integration and increase the impact of unsteady aeroelasticity in the aircraft design process, efficient derivative computation for unsteady aerodynamics and flutter speed are necessary. Indeed, gradient based optimization is one of the most popular approach for aircraft multidisciplinary design and optimization (MDO), and the only viable solution when the number of design variables is extremely high, like in large scale MDO. This approach strongly rely on the accuracy of the derivative of the objective and constraint function with respect to design variables.
In literature, several works deal with the definition of the flutter speed, or flutter constraint, derivative. These works differs for the level of fidelity of the structural model, of the aerodynamic model and the design variables considered in the differentiation. In [6] a modified strip theory is used to compute the unsteady aerodynamic foraces in frequency domain, whereas the wing structure is modeled as an equivalent plate. The low fidelity of both aerodynamic and structural model allows to obtain an analytic expression for the flutter speed derivative with respect to wing planform parameters, such as aspect ratio, area, taper ratio and sweep angle. In [7], the accuracy of the previous aerodynamic model is increased, by correcting the strip theory with finite span effects. Ref. [8] uses the same analytic approach substituting the strip theory with the piston theory in order to study supersonic flow conditions.
In [9] the level of fidelity of the aerodynamic model is increased by using the doublet lattice method (DLM), whereas the wing structure is modeled with a beam-based finite element method. The use of the finite state modeling for the aerodynamic term allows to use state space analysis to solve the aeroelastic equation, and hence to obtain the analytic expression for the derivative of the flutter speed. However, the increased fidelity of the aerodynamic model prevents the use wing planform parameter as design variable, only structural parameter, such as bending and torsional stiffness are considered. Indeed, with the DLM, in order to obtain the flutter speed derivative with respect to wing planform parameter, the derivative of the structural modal shapes cannot be neglected, as done in [9].
Ref. [10] describes the NeoCASS framework for conceptual aero-structural sizing of the complete aircraft configuration. DLM, as well as a RANS based reduced order model, are available for the aerodynamic analysis. Both fuselage and wing structure are modeled with a stick finite element model, in which all the parameter of the section, like skin, frames and spar, are used to define the section stiffness characteristics. The framework allows the user to perform structural optimization using gradient based algorithm. Also in this case, only derivative of flutter speed with respect to structural parameters are considered.
A detailed shell element wing structural model is used in [11] to perform topological opti-

mization, and the aerodynamic analysis is carried out with DLM. The non-iterative procedure proposed in [12] is used to solve the *p-k* form of the flutter equation. Again, only the flutter speed derivative with respect to structural parameters is computed, therefore the derivative of the structural modal shapes are neglected.
A similar approach is used in [13, 14], where DLM is employed for the aerodynamic analysis, and the structural modeling and analysis is carried out using the TACS software [15], a FEM solver specialized for thin-walled composite structures. As in [11], the flutter analysis is performed with a non iterative *p-k* procedure. Planform parameters as well as structural parameters are considered as design variable for the flutter speed derivative computation, thus the derivative of the structural mode shapes are included in the differentiation procedure.

The work here presented is part of an overall framework, aiming to enhance the aircraft early design stages for conventional and unconventional configurations by physics based analyses, for instance by accounting for static and dynamic aeroelastic constraints. Here, the unsteady aerodynamic analysis is carried out with the boundary element method developed by Morino [16], and able to consider generic 3D body shapes. The aeroelastic equation is solved using a state space approach resulting in a twofold benefit. First, the form of the aeroelastic equation is mathematically valid also far from the flutter point. Second, the complex root finding procedure, used in the *p-k* method to solve the frequency matching problem, is replaced by a standard root locus method. Moreover, the finite state aerodynamic modeling, necessary for the state space approach, allows us to obtain flutter speed and flutter frequency derivative analytically.
The unsteady aerodynamics is differentiated with respect to wing planform parameters. Therefore, we cannot neglect the dependency of the modal shapes on the design variables, and they are differentiated accordingly exploiting the method presented by Cardani and Mantegazza in [17].
The developed unsteady aeroelastic module is suitable for a collaborative and multidisciplinary aircraft design process. In order to foster the integration among the different disciplinary modules, the central data schema CPACS [18] is used as standard input-ouput data format. The tool is also accessible via RCE [19], the DLR's distributed environment in which the design process is implemented. These two features, together with the complete automatization of the analysis procedure, make the unsteady aeroelastic module suitable for large collaborative MDO process.

In Section 2 we describe the implemented analysis method, such us the boundary element method for aerodynamic, and the state space approach for the flutter analysis. In Section 3 the definition and implementation of the flutter speed derivative is discussed and results are compared with finite difference results. Finally, in Section 4 the entire procedure is applied to the Goland wing use case, a typical test case for flutter analysis.

2 THE UNSTEADY AEROELASTIC MODULE

2.1 Morino's Method

The current state of the art for accurate aeroelastic instability prediction consists of time-marching coupled CFD-CSD simulations. The small size of the time steps, required to obtain reliable results, increases significantly the computational cost of the analysis, making it not always suitable for preliminary aircraft design, where time constraint and available computational resources may postpone the deployment of CFD to later design stages. Indeed, the standard flutter prediction method in the industrial environment, for the prelimnary phase, is based on a flat surface linear aerodynamic model, the doublet-lattice method (DLM), developed by Albano and Rodden [20]. These method abstracts the wings to lifting surfaces, which can be flat [21] or twisted [22], whereas the fuselage, if considered, is treated with dedicated elements

for 3D non-lifting body. The low computational cost compensates for the low fidelity of the model, and the reliability is increased correcting the aerodynamic influence coefficients (AIC) with wind tunnel experimental data. For an optimization process this data are not available, hence the need to push forward the fidelity of the aerodynamic analysis without increasing the computational cost.

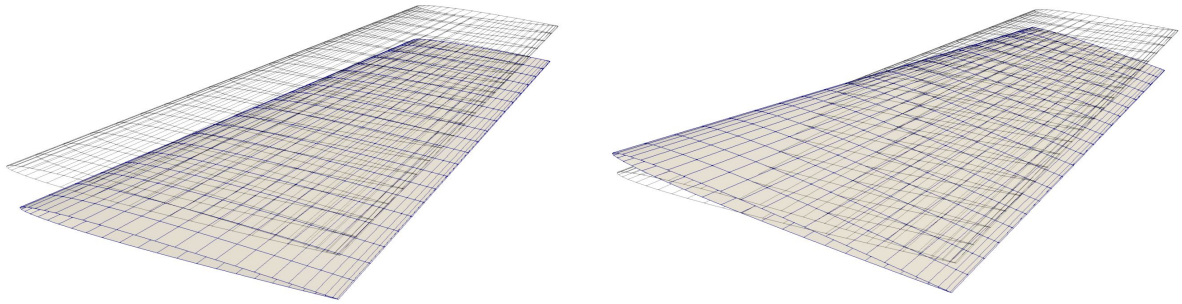

Figure 1: **Onera M6 wing model with 500 body panels. The plunging-pitching motion shapes are also represented in the left and right sub-figure respectively.**

Here, the boundary element method proposed by Morino in [16] is implemented for the frequency domain aerodynamic analysis of 3D bodies. Morino's method is based upon the integral equation obtained applying the Green's function theorem to the small perturbation equation, and can be used for steady as well as unsteady aerodynamic analysis, for subsonic as well as supersonic flow. Here, only the subsonic incompressible model is implemented.
Morino's boundary element method and DLM solve the same field equation, the small perturbation equation, but they strongly differ in terms of geometrical fidelity of the boundary condition. It has also been proved by Morino in [23] that, for a null-thickness body, his theory reduces properly to the lifting surface theory of the standard DLM. One of the contribution of this paper is the extensive comparison between DLM and Morino's method, carried out to validate our implementation.

With this method, arbitrary complex 3D bodies are treated in an unified manner, reducing the effort and increasing the robustness of the model generation phase and of the aero-structural mapping as well. For an MDO environment suitable for a large range of aircraft configurations, conventional as well as unconventional, this is a key feature of the aeroelastic analysis module. Besides implementation aspects, the increased geometrical fidelity of Morino's method has been proved to be necessary to capture important unsteady aerodynamic effects, like in-plane motion aerodynamic effects and local fuselage-wing interference.
Finally, it is important to highlight that Morino's method has a computational cost comparable with DLM. With respect to the latter, additional panels are needed to cover the aircraft outer mold line, and also the wake needs to be modeled with panels. However, the performed convergence studies suggest that the necessary number of panels and length of the wake do not downgrade the computational performances of the method. For the Onera M6 wing use case, 500 body panels and 500 wake panels are sufficient to have a converged solution, see figures 1 and 2, and approximately 3 seconds are needed to compute one element of the GAF matrix for one value of reduced frequency, on a 4×2.70 GHz cores machine. Note that, the most expensive part of the computation is the model generation, changing mode shapes or value of reduced frequency only affects the boundary condition. Indeed, for the same use case nearly the same time (approximately 4 seconds) is needed to compute a 5×5 GAF matrix for 10 values of reduced frequency.

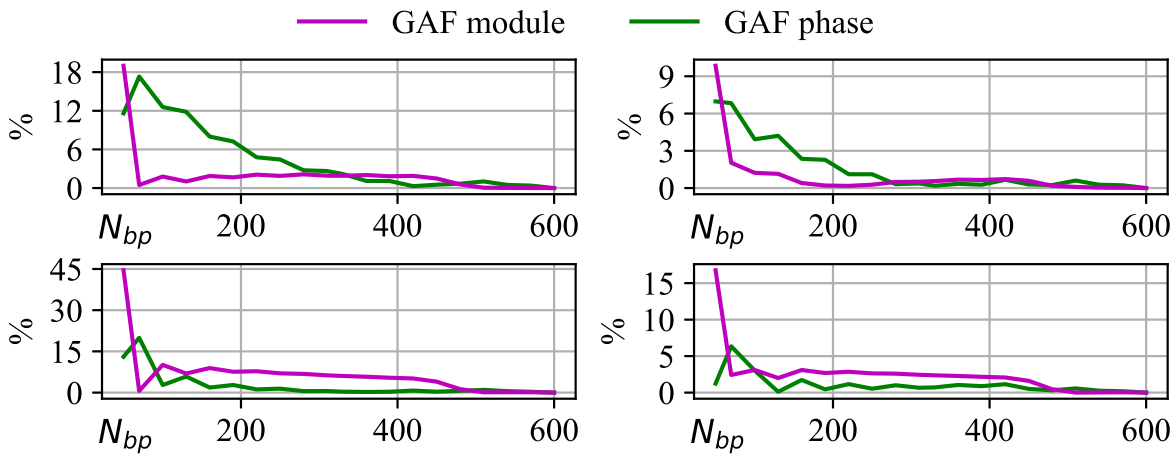

(a) Number of body panels N_{bp}

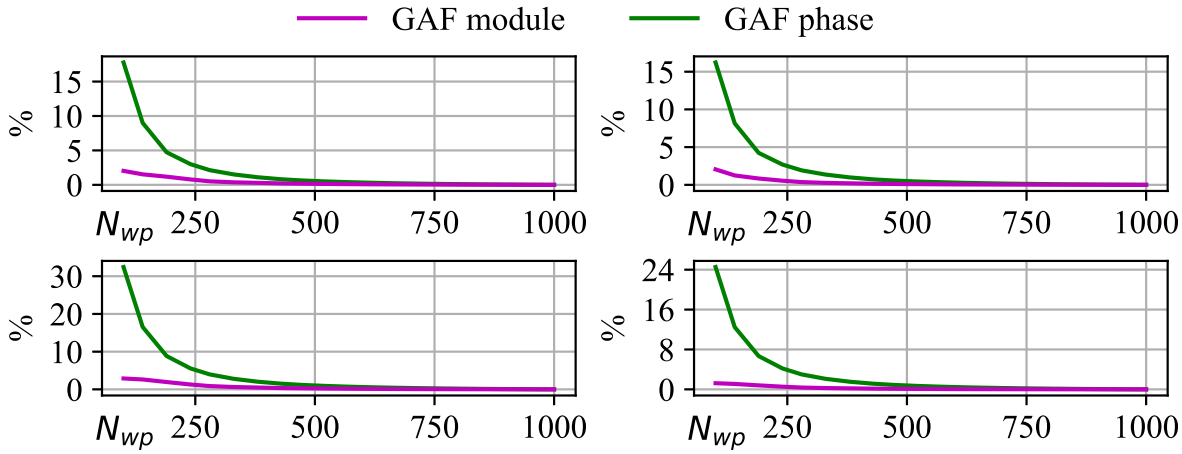

(b) Number of wake panels N_{wp}

Figure 2: **Converge studies on the number of body (a) and wake (b) panels. Use case: Onera M6 wing. The** 2×2 **GAF matrix is calculated for the plunging-pitching motion depicted in figure 1 and a reduced frequency** $k = 0.76$**.**

2.1.1 Comparison between Morino's Method and Doublet Lattice Method

Validation studies have been already presented by the authors in [24]. Our implementation of Morino's method is compared to Theodorsen's theory and the DLM implemented in NASTRAN MSC. Nevertheless, by using a commercial code the comparison has been carried out only for the top-level results, leaving open the possibility of lower-level bugs.
Here, we present a comparison between the implemented Morino's method and the DLM implementation described by Demasi in [25]. The chosen use case is the Onera M6 wing already used for the convergence study. The 6×6 GAF matrix elements are compared for 20 values of reduced frequency ranging from 0 to 2, the typical interval for flutter analysis. We condider 6 motion shapes: plunging, pitching and the first 4 structural modes, see figure 3.

As can be seen from figure 4, a good agreement is found among the two methods. The higher discrepancy is observed for the 3^{rd} structural mode, while for the other motion shapes the two curves are practically overlapping. It has been also observed a decrease of the discrepancy due to a decrease in the thickness to chord ratio.
The comparison continues on lower-level variables the pressure jump across the lifting surface

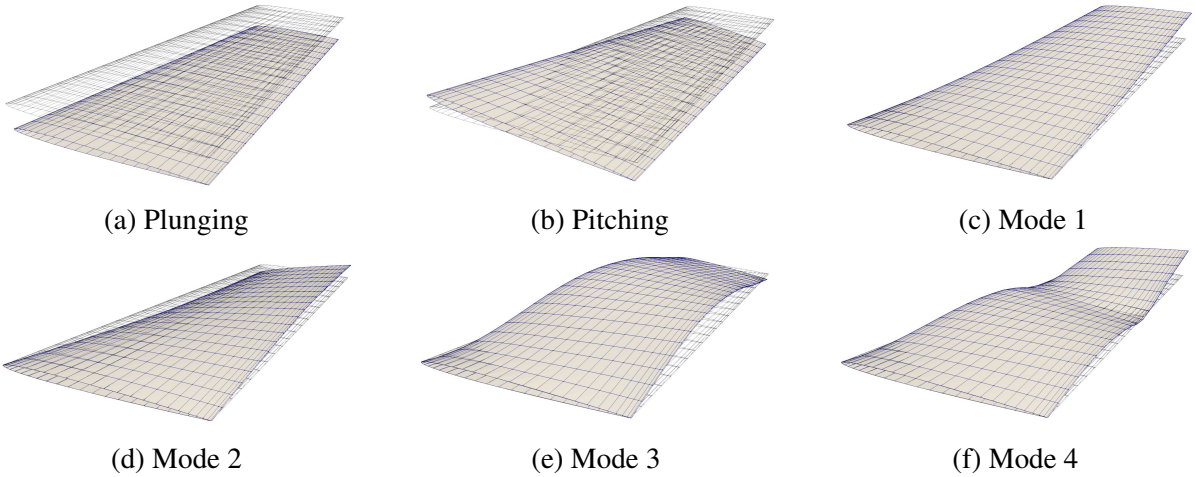

(a) Plunging (b) Pitching (c) Mode 1

(d) Mode 2 (e) Mode 3 (f) Mode 4

Figure 3: **The** 6 **displacement shapes used for the comparison between Morino's method and doublet lattice method.**

ΔC_p. In order to carry out this comparison, the 3D model is reduced to the equivalent flat model using averaging the contribution of upper and lower panels. Figure 5 shows a good agreement also on these lower-level variables for rigid body as well as structural modal motions.

2.2 Finite State Aerodynamic

In linear flutter analysis [1] the Laplace transform of the generalized aerodynamic force vector, $\boldsymbol{f}(s)$, is expressed as

$$\boldsymbol{f}(s) = \boldsymbol{Q}(sl/U_\infty)\boldsymbol{q} \tag{1}$$

where $\boldsymbol{Q}$ is the so called generalized aerodynamic forces matrix (GAF), and is a non linear function of s and U_∞ only through the complex reduced frequency $p := sl/U_\infty$. Note that, except some very simple cases like the classic Theodorsen two-dimensional theory, it is not possible to obtain the analytic expression of $\boldsymbol{Q}(p)$, which is instead evaluated numerically on a finite number of sampling points. In fact, the methods used for the evaluation of $\boldsymbol{Q}(p)$ are able to compute the unsteady aerodynamic forces only for harmonic oscillation motion, that is for $p = ik$, where k is the reduced frequency. Then, $\boldsymbol{Q}(p)$ is the analytic continuation of $\boldsymbol{Q}(ik)$. As pointed out in [26] comment 4: "if two analytic function coincide over the imaginary axis, they will coincide over the whole domain of analyticity", meaning that the finite state approach provides an approximation of GAF matrix that is valid also outside the imaginary axis, or, in other words, far from the standard definition of the flutter point.

This is particularly valuable when advanced definition of the flutter point are used, such as the one proposed in [27]. In order to reduced the hard discontinuities of flutter speed due to mode switching or mode hopping, the flutter point is defined as the intersection of the damping curve with an *ad-hoc* function of the free stream speed, $G(U_\infty)$, instead of the classic zero-damping axis. Therefore, as clarified by figure 6, the flutter point is now outside the pure imaginary axis, and hence it is in this region that the prediction has to be accurate.

In the finite state aerodynamic approach, $\boldsymbol{Q}$ is approximated by a rational expressions in which the non-linear dependency of Q on p appears explicitly. Then, the aeroelastic equation can be

[1] With the term *linear* we mean that the aerodynamic forces depend linearly on the Lagrangian coordinates representing the surface motion. Instead, the non linear relation of the aerodynamic term with respect to the free-stream speed and the frequency of oscillation is fully included.

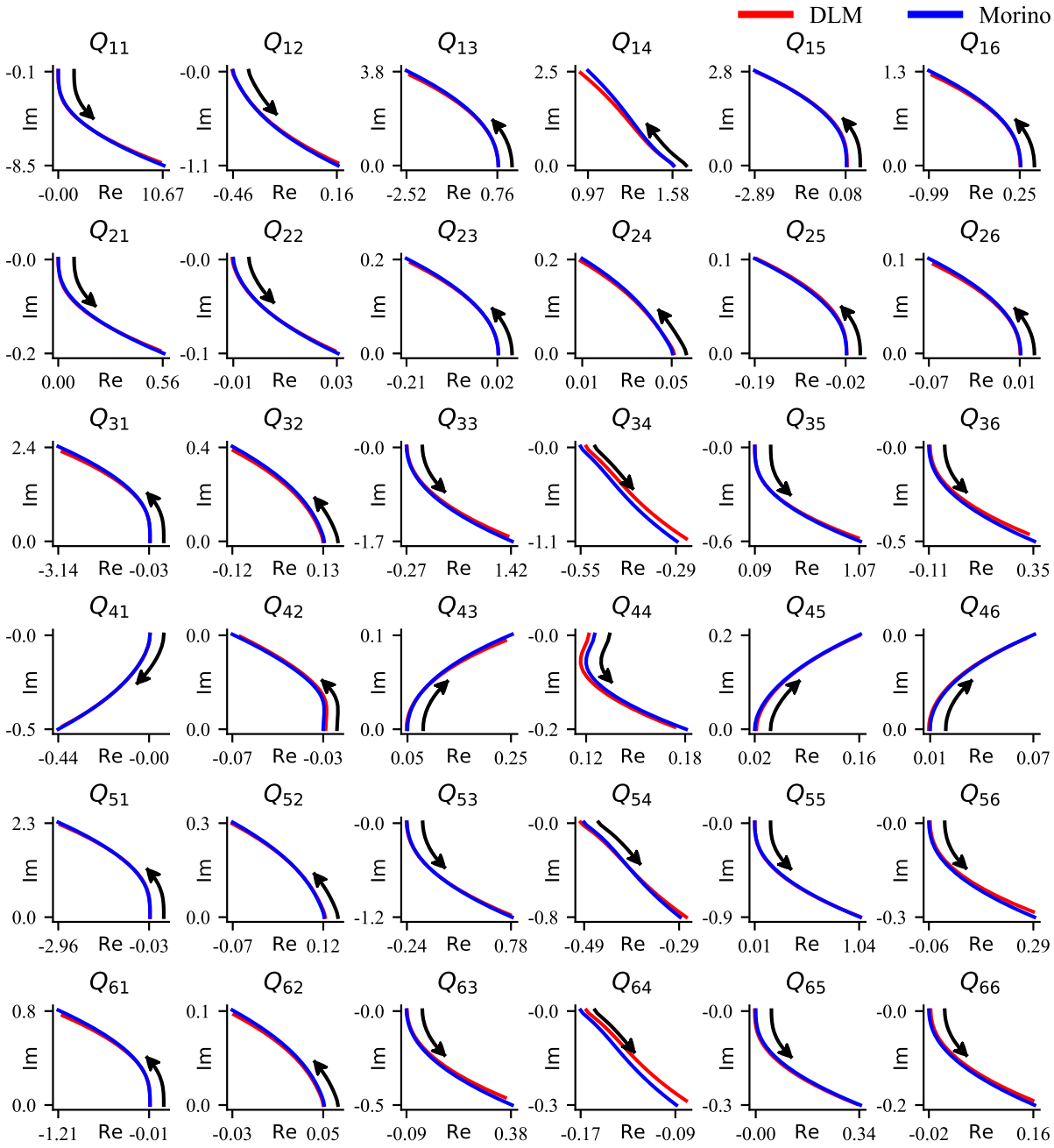

Figure 4: **Comparison between Morino's method and DLM predicted GAF. The elements of the GAF matrix are plotted for increasing values of the reduced frequency, from** 0 **to** 2**, according to the black arrow.**

rewritten, in time domain, as $\boldsymbol{Ax} = \dot{\boldsymbol{x}}$, making possible to replace the *p-k* method, with a simple root locus method, see subsection 2.3.

The finite state approach is also advantageous for control analysis and loads studies, such as maneuver and gust analysis, see for example [28] on optimal control design, [29] on free-body aeroelasticity. Further, the analytic expression of the $Q - p$ dependency allows us to obtain the analytic derivative of Q with respect to the reduced frequency k, as necessary to obtain the flutter speed derivative, see Section 3.

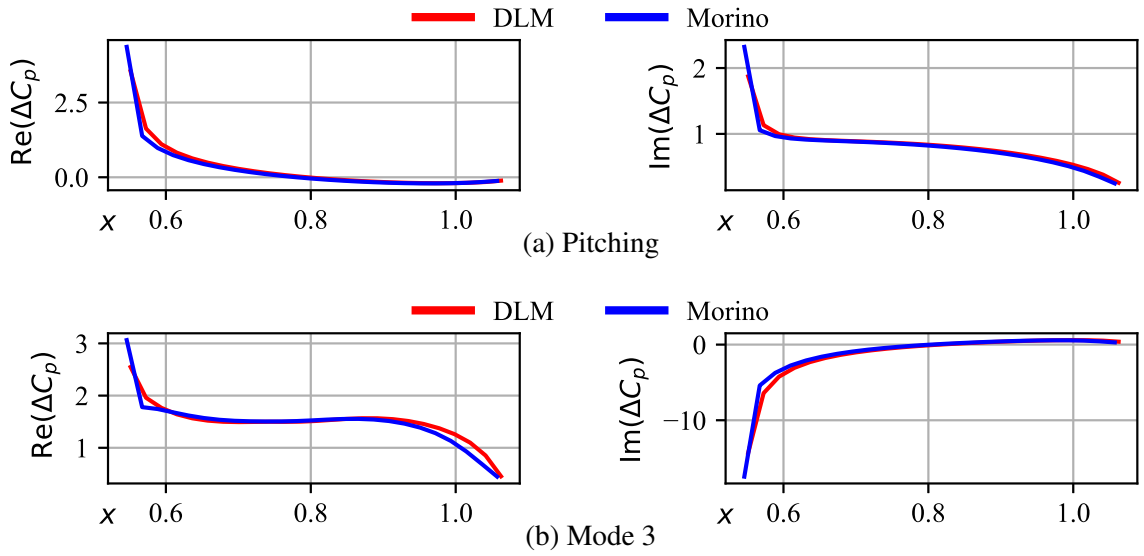

Figure 5: **Comparison between Morino's method and DLM predicted pressure jump ΔC_p. The chord-wise distribution is plotted for a section at $3/4$ of the semi-span, and for $k = 0.88$.**

Usually the $\boldsymbol{Q}(p)$ is evaluated numerically by means of low or medium fidelity aerodynamics methods like DLM or the Morino's method implemented here. However, although not exploited in this work, the methods presented in this subsection, in subsection 2.3, and part of the method presented in Section 3 can also be applied to non-linear aerodynamics model once GAF are provided, see for example [30] and [31].

2.2.1 RFA and MFA Finite State Model

Two different finite state approximations are implemented: the rational function approximation (RFA) developed by Roger in [32], and the matrix fraction approximation (MFA) proposed by Morino etal. in [26].

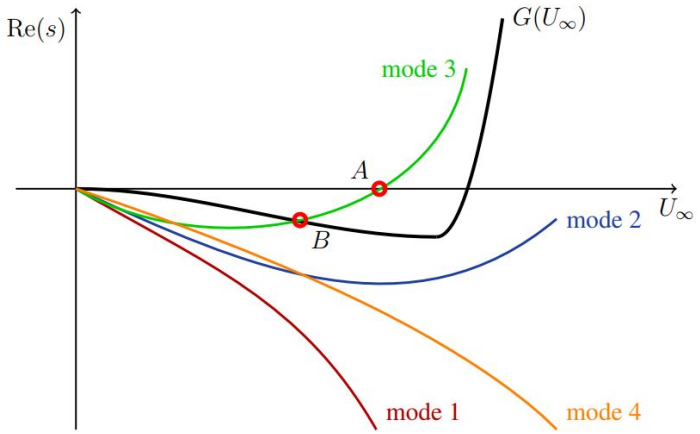

Figure 6: **Classical flutter point definition A, and definition proposed in [27], B.**

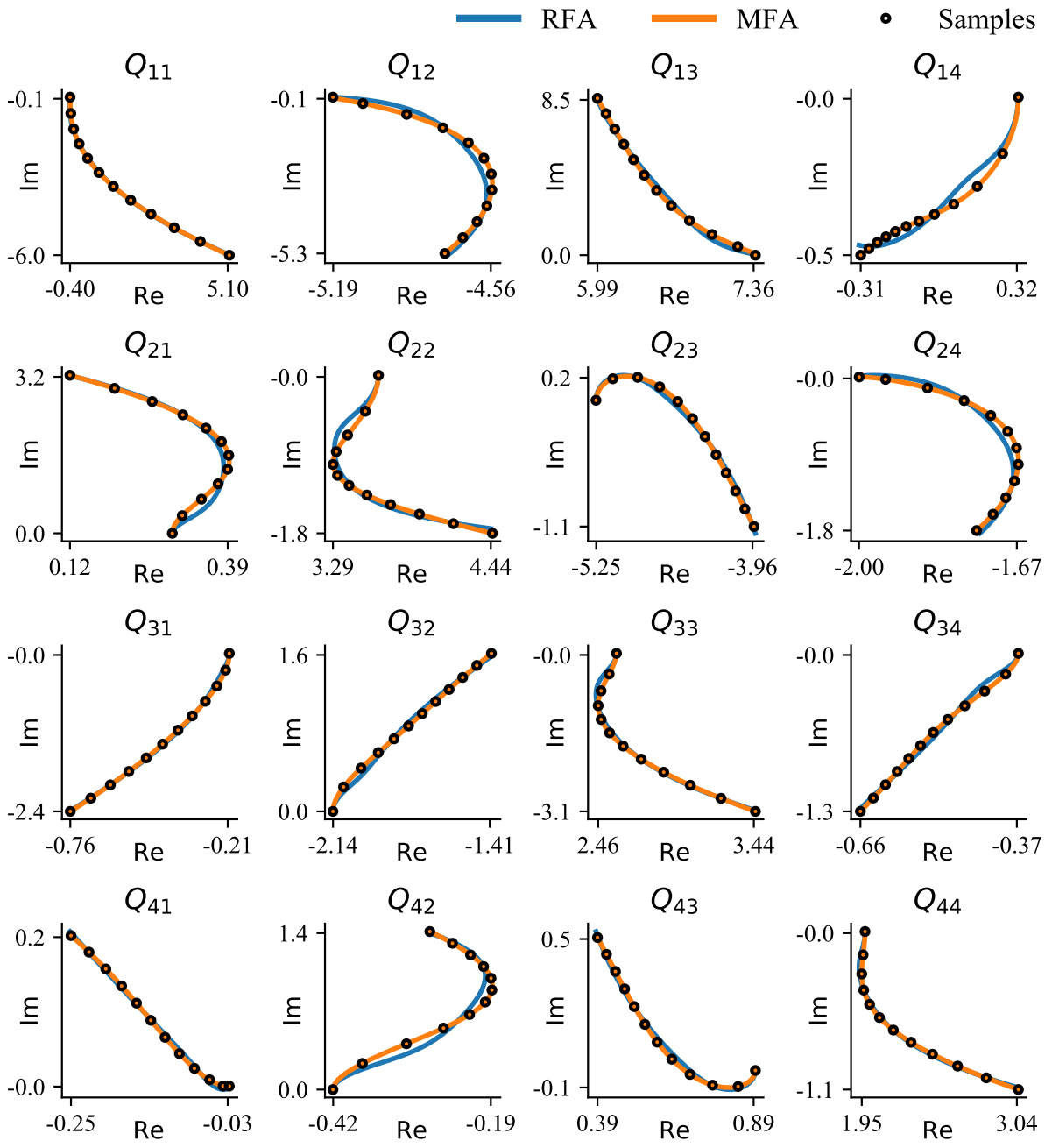

Figure 7: **Comparison between MFA and RFA models using 2 poles. The elements of the GAF matrix approximation are plotted for increasing values of the reduced frequency, from 0 to 2. The use case is the 15 degree swept back wing of the HA145E NASTRAN example, the first 4 structural modes are considered.**

In Roger's model the GAF matrix is approximated with a quadratic polynomial plus lags terms:

$$\boldsymbol{Q}(p) \approx \hat{\boldsymbol{Q}}(p) := \boldsymbol{E}_0 + \boldsymbol{E}_1 p + \boldsymbol{E}_2 p^2 + \sum_{i=1}^{M} \frac{p}{p+\beta_i} \boldsymbol{E}_{i+2} \tag{2}$$

where the poles β_i are real, positive and with the same order of magnitude of p. Morino's model eliminates the arbitrariness in the choice of the poles, approximating the GAF matrix as

a fraction of matrix polynomials.

$$\boldsymbol{Q}(p) \approx \hat{\boldsymbol{Q}}(p) := \left(\sum_{i=0}^{M} \boldsymbol{D}_i p^i\right)^{-1} \left(\sum_{i=0}^{M+2} \boldsymbol{N}_i p^i\right) \tag{3}$$

The accuracy of the approximation increases with increasing the number of poles, M in both eq. (2) and (2), which is equal to the size of the state space system. The approximation matrices, $\boldsymbol{E}_i$, $\boldsymbol{D}_i$ and $\boldsymbol{N}_i$, are in both model obtained solving a least square problem in which the distance from the GAF samples, $\boldsymbol{Q}(ik)$, is minimized.

Figure 7 shows that, using the same numbers of poles, Morino's model is significantly more accurate than Roger's one. For instance, in [33] it is used to approximate the complex aerodynamics of rotors. For the Theodorsen's use case we compute the integral of the error between the finite state models and the analytic solution over the range of considered reduced frequency, see table 1.

Table 1: **Comparison between MFA and RFA models using** 2 **poles and** 11 **sampling points.**

	Error
Roger's model	2.96×10^{-4}
Morino's model	3.54×10^{-5}

2.3 State Space Flutter Analysis

We consider the aeroelastic equation expressed in the following form[2],

$$\left(\boldsymbol{M}s^2 + \boldsymbol{C}s + \boldsymbol{K}\right)\boldsymbol{q} = q_D \boldsymbol{Q}\left(sl/U_\infty\right)\boldsymbol{q} \tag{4}$$

where $q_D := 1/2\rho U_\infty^2$ is the dynamic pressure. By using one of the finite state approximations proposed in subsection 2.2 we obtain the sought form of the aeroelastic system of equations. Here, we report only the system of equations obtained with the MFA model, since our implementation is slightly differ from the one proposed in [26], and the RFA version is the most popular.
Substituting eq. (3) into eq. (4) we obtain the following aeroelastic system of equations,

$$\begin{cases} \frac{U_\infty^2}{l^2}\boldsymbol{M}\ddot{\boldsymbol{q}} + \frac{U_\infty}{l}\boldsymbol{C}\dot{\boldsymbol{q}} + \boldsymbol{K}\boldsymbol{q} + \frac{U_\infty^2}{l^2}\left(\boldsymbol{D}_{M-1}\boldsymbol{M}\dot{\boldsymbol{q}} + \boldsymbol{D}_{M-2}\boldsymbol{M}\boldsymbol{q}\right) + \frac{U_\infty}{l}\boldsymbol{D}_{M-1}\boldsymbol{C}\boldsymbol{q} = \\ \qquad\qquad q_D\left(\boldsymbol{N}_M\boldsymbol{q} + \boldsymbol{N}_{M+1}\dot{\boldsymbol{q}} + \boldsymbol{N}_{M+2}\ddot{\boldsymbol{q}}\right) + \boldsymbol{v}_{M-1} \\ \dot{\boldsymbol{v}}_{M-1} + \frac{U_\infty^2}{l^2}\boldsymbol{D}_{M-3}\boldsymbol{M}\boldsymbol{q} + \frac{U_\infty}{l}\boldsymbol{D}_{M-2}\boldsymbol{C}\boldsymbol{q} + \boldsymbol{K}\boldsymbol{D}_{M-1}\boldsymbol{q} = q_D\boldsymbol{N}_{M-1}\boldsymbol{q} + \boldsymbol{v}_{M-2} \\ \dots \\ \dot{\boldsymbol{v}}_2 + \frac{U_\infty^2}{l^2}\boldsymbol{D}_0\boldsymbol{M}\boldsymbol{q} + \frac{U_\infty}{l}\boldsymbol{D}_1\boldsymbol{C}\boldsymbol{q} + \boldsymbol{D}_2\boldsymbol{K}\boldsymbol{q} = q_D\boldsymbol{N}_2\boldsymbol{q} + \boldsymbol{v}_1 \\ \dot{\boldsymbol{v}}_1 + \frac{U_\infty}{l}\boldsymbol{D}_0\boldsymbol{C}\boldsymbol{q} + \boldsymbol{D}_1\boldsymbol{K}\boldsymbol{q} = q_D\boldsymbol{N}_1\boldsymbol{q} + \boldsymbol{v}_0 \\ \dot{\boldsymbol{v}}_0 + \boldsymbol{D}_1\boldsymbol{K}\boldsymbol{q} = q_D\boldsymbol{N}_0\boldsymbol{q} \end{cases}$$

where the over-dot represents the differentiation with respect to $U_\infty t/l$. By applying the Laplace transform the eigenvalue problem system is obtained: $\boldsymbol{A}(U_\infty)\boldsymbol{x} = p\boldsymbol{x}$, where $\boldsymbol{x}$ is the vector of states containing physical as well as added aerodynamic states.

[2]Instead, in the *p-k* method the aeroelastic equation is expressed as $\left(\boldsymbol{M}s^2 + \boldsymbol{C}s + \boldsymbol{K}\right)\boldsymbol{q} = q_D\boldsymbol{Q}\left(ik\right)\boldsymbol{q}$, which is mathematically inconsistent for $\mathrm{Re}(s) \neq 0$, since $\boldsymbol{Q}\left(ik\right)$ is calculated only for non-damped harmonic oscillations.

The aeroelastic state space system is solved for a set of free stream speed values, U_∞, ranging from null speed to the maximum speed in the flight envelope. In general the order of the eigenvalues corresponding to adjacent speed values is not the same, hence the need for adequate mode tracking techniques. We implemented the modal assurance criterion (MAC) proposed by Van Zyl in [34]. Note that, since the GAF matrix is complex, the aeroelastic eigenvectors are complex as well, and the standard MAC are not accurate enough. For each speed value different from zero, each eigenvector is compared to all the eigenvectors obtained at the previous speed value. The highest value of the van Zyl's correlation function indicates the matched couple of eigenvectors. Once all the states have been tracked, the spurious ones can be easily discarded knowing that, for null speed, the physical eigenvalues have null real part and imaginary part equal to the correspondent structural natural frequency.

2.4 Simplified Finite Element Model and Mode Mapping

Focus of this work is the definition and implementation of a flutter speed differentiation procedure, in which wing planform parameters are used as design variables, and the unsteady aerodynamic forces are obtained with Morino's method. Hence, the structural model is kept as simple as possible, and the integration with advanced finite element structural model like the open source TACS [15] is planned for the near future. Due to the low fidelity of the structural model, some of the advantages connected to the 3D capability of Morino's method cannot be highlighted by this work. However, we tackle the most important and difficult part of the structural analysis: the differentiation of the structural modal shapes with respect to the geometrical parameters, such as the wing planform ones, see Section 3.

The implemented structural model is a simplified beam-based FEM. Each node has only 3 degrees of freedom, namely: the displacement and rotation associated to the primary bending, and the rotation due to torsion; since these two are the most important modes for flutter analysis in simple aeroelastic model, as the one considered in this work.

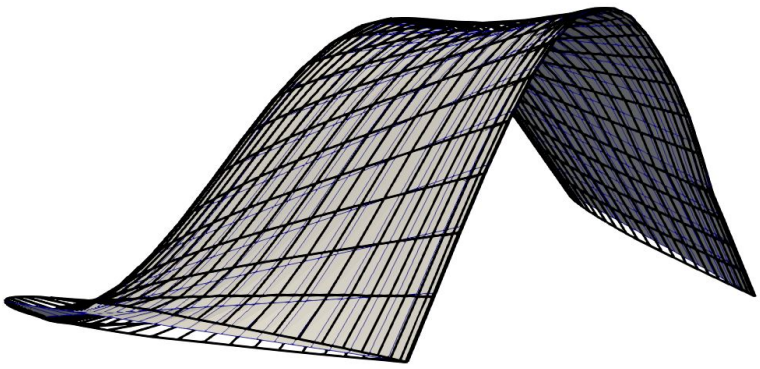

Figure 8: **Mapping of the 2^{nd} bending mode on the 3D aerodynamic grid (black wireframe), for the Onera M6 wing**

The mapping of structural modal displacements onto the aerodynamic grid is based on the radial basis function method described by Beckert and Wendland [35] or Rendall and Allen [36], and the *in-house* implementation described in [37] is used. In order to decrease the discrepancy between the 1D structural grid and the 3D aerodynamic grid, additional mass-less points are added on both trailing and leading edges, and are rigidly connected to the corresponding beam node to correctly map the displacements due to torsional rotations, see figure 8.

3 DIFFERENTIATION PROCEDURE

Equation (4) is manipulated in order to obtain a more compact expression in which only the dependencies on design variables vector $\boldsymbol{t}$, complex frequency s, and free-stream speed U_∞ are highlighted.

$$[\boldsymbol{A}(\boldsymbol{t}, U_\infty, s) - s\boldsymbol{B}(\boldsymbol{t})]\,\boldsymbol{q} = 0 \tag{5}$$

where

$$\boldsymbol{A} = \begin{bmatrix} \boldsymbol{0} & \boldsymbol{I} \\ \rho_\infty U_\infty^2/2\boldsymbol{Q}(sl/U_\infty, \boldsymbol{t}) - \boldsymbol{K}(\boldsymbol{t}) & -\boldsymbol{C}(\boldsymbol{t}) \end{bmatrix}$$
$$\boldsymbol{B} = \begin{bmatrix} \boldsymbol{I} & \boldsymbol{0} \\ \boldsymbol{0} & \boldsymbol{M}(\boldsymbol{t}) \end{bmatrix}$$

With the method described in subsection 2.3 we compute the n-th right and left eigenvectors, $\boldsymbol{u}^{(n)}$ and $\boldsymbol{v}^{(n)}$, and n-th eigenvalue, $s^{(n)}$, where $n = [1, \dots N_s]$ and N_s is the number of chosen Lagrangian coordinates, we proceed with the eigensensitivity analysis differentiating eq.(5) with respect to the design variables.

First, we multiply by the left eigenvector.

$$\boldsymbol{v}^{(n)^T}\left[\boldsymbol{A}(\boldsymbol{t}, U_\infty, s^{(n)}) - s^{(n)}\boldsymbol{B}(\boldsymbol{t})\right]\boldsymbol{u}^{(n)} = 0 \tag{6}$$

Then we differentiate with respect to one of the design variable[3], t. For the sake of simplicity we drop the dependency from $\boldsymbol{t}$, U_∞ and $s^{(n)}$.

$$\left(\frac{\mathrm{d}\boldsymbol{v}^{(n)}}{\mathrm{d}t}\right)^T [\boldsymbol{A} - s^{(n)}\boldsymbol{B}]\boldsymbol{u}^{(n)} + \boldsymbol{v}^{(n)^T}[\boldsymbol{A} - s^{(n)}\boldsymbol{B}]\frac{\mathrm{d}\boldsymbol{u}^{(n)}}{\mathrm{d}t} + \\ + \boldsymbol{v}^{(n)^T}\left[\frac{\partial \boldsymbol{A}}{\partial t} + \frac{\partial \boldsymbol{A}}{\partial U}U_t + \frac{\partial \boldsymbol{A}}{\partial s}s_t^{(n)} - s_t^{(n)}\boldsymbol{B} - s^{(n)}\frac{\partial \boldsymbol{B}}{\partial t}\right]\boldsymbol{u}^{(n)} = 0$$

Reordering the above equation with respect to the unknown U_t and $s_t^{(n)}$, and exploiting the definition of right and left eigenvector yields

$$\boldsymbol{v}^{(n)^T}\frac{\partial \boldsymbol{A}}{\partial U}\boldsymbol{u}^{(n)}U_t + \boldsymbol{v}^{(n)^T}\left[\frac{\partial \boldsymbol{A}}{\partial s} - \boldsymbol{B}\right]\boldsymbol{u}^{(n)}s_t^{(n)} = \boldsymbol{v}^{(n)^T}\left[\frac{\partial \boldsymbol{A}}{\partial t} - s^{(n)}\frac{\partial \boldsymbol{B}}{\partial t}\right]\boldsymbol{u}^{(n)} \tag{7}$$

Considering the real and the imaginary part of eq.(7) we obtain 2 independent equations in 3 unknown: U_t, $\mathrm{Re}(s_t^{(n)})$ and $\mathrm{Im}(s_t^{(n)})$. In order to close the system, we have to introduce another equation involving U_∞ and $s^{(n)}$. We can consider two different cases.

1. We are interested in the derivative of the aeroelastic frequency, $s^{(n)}$, for a specific value of the flight speed, U_∞. Then, all the derivative involving U_∞ are null and we have 2 equation in 2 unknown $\mathrm{Re}(s_t^{(n)})$ and $\mathrm{Im}(s_t^{(n)})$.
2. We are interested in the derivative at the flutter point, hence $\mathrm{Re}(s^{(n)}) = 0$, and we have 2 equation in 2 unknown U_t and $\mathrm{Im}(s_t^{(n)})$. This procedure apply also the definition of flutter point mentioned in subsection 2.2. In this case the system of equation is closed by the additional equation $\mathrm{Re}(s^{(n)}) = G(U_\infty)$.

[3]The entire vector of design variables can be considered, but the following procedure and results are still valid

Next, we compute the matrix derivative with respect to the design variable.

$$\frac{\partial \boldsymbol{A}}{\partial t} = \begin{bmatrix} \mathbf{0} & \mathbf{0} \\ \frac{1}{2}\rho_\infty U_\infty^2 \frac{\partial \boldsymbol{Q}}{\partial t} - \frac{\partial \boldsymbol{K}}{\partial t} & -\frac{\partial \boldsymbol{C}}{\partial t} \end{bmatrix} \tag{8}$$

$$\frac{\partial \boldsymbol{A}}{\partial U} = \begin{bmatrix} \mathbf{0} & \mathbf{0} \\ \rho_\infty U_\infty \boldsymbol{Q} - \frac{1}{2}\rho_\infty s^{(n)} l \frac{\partial \boldsymbol{Q}}{\partial p} & \mathbf{0} \end{bmatrix} \tag{9}$$

$$\frac{\partial \boldsymbol{A}}{\partial s} = \begin{bmatrix} \mathbf{0} & \mathbf{0} \\ \frac{1}{2}\rho_\infty U_\infty l \frac{\partial \boldsymbol{Q}}{\partial p} & \mathbf{0} \end{bmatrix} \tag{10}$$

$$\frac{\partial \boldsymbol{B}}{\partial t} = \begin{bmatrix} \mathbf{0} & \mathbf{0} \\ \mathbf{0} & \frac{\partial \boldsymbol{M}}{\partial t} \end{bmatrix} \tag{11}$$

Subsection 3.2 shows the procedure for the derivative of the structural matrices, $\boldsymbol{M}$, $\boldsymbol{C}$ and $\boldsymbol{K}$, as well as the derivative of the modal shapes with respect to the design variable t. Section 3.1 concerns the partial derivative of the aerodynamic matrix, $\boldsymbol{Q}$, with respect to t. For the derivatives of $\boldsymbol{Q}$ with respect to the complex reduced frequency p, we exploit the finite state aerodynamic approximation. Differentiating eq.(3) with respect to p we have

$$\dot{\boldsymbol{Q}}(p) = \boldsymbol{D}(p)^{-1}\dot{\boldsymbol{N}}(p) - \boldsymbol{D}(p)^{-1}\dot{\boldsymbol{D}}(p)\boldsymbol{Q}(p) \tag{12}$$

where

$$\dot{\boldsymbol{N}}(p) = \sum_{i=0}^{M+2} i p^{i-1} \mathbf{N}_i \quad \text{and} \quad \dot{\boldsymbol{D}}(p) = \sum_{i=0}^{M} i p^{i-1} \mathbf{D}_i \tag{13}$$

Finally, the procedure to compute the flutter speed derivative can be summarized in the following steps.

1. Compute, with the preferred method, flutter speed U_F, flutter frequency ω_F, flutter right and left eigenvectors $\boldsymbol{u}_F$ and $\boldsymbol{v}_F$, as they appear in eq.(5). We use the root locus method, but the procedure does apply to any other method, like the *p-k* method for example.
2. Compute the partial derivative of the matrices, $\frac{\partial \boldsymbol{A}}{\partial t}$, $\frac{\partial \boldsymbol{A}}{\partial U}$, $\frac{\partial \boldsymbol{A}}{\partial s}$ and $\frac{\partial \boldsymbol{B}}{\partial t}$, with eqs. (8) to (11) replacing U_∞ with U_F and $s^{(n)}$ with $i\omega_F$.
3. Compute flutter speed derivative, $U_{F,t}$, and flutter frequency derivative , $\omega_{F,t}$, with eq.(7) using U_F and $i\omega_F$ instead of U_∞ and $s^{(n)}$.

3.1 Derivative of the Generalized Aerodynamic Forces Matrix

Each element of the generalized aerodynamic forces matrix, Q_{hk}, represent the work done by the aerodynamic pressure due to the k-th shape motion on the h-th displacement shape.

$$Q_{hk} = \iint_{S_B} \phi^h \cdot \boldsymbol{n} \left[-2 \left(ik/l \mu^k + \left(\mu_\xi^k \boldsymbol{l} + \mu_\eta^k \boldsymbol{m} + \sigma^k \boldsymbol{n} \right) \cdot \boldsymbol{i} \right) \right] \mathrm{d}S \tag{14}$$

where ϕ^h is the h-th shape function, σ^k and μ^k are the aerodynamic unsteady normal-wash (see eq.(15)) and potential associated to the k-th deformation shape, S_B indicates the body surface, and (ξ, η) the relative surface coordinates system. The aerodynamic potential is obtained solving the linearized potential flow equation:

$$\begin{cases} \nabla^2 \mu^k = 0 & \text{in } \Omega \\ \dfrac{\partial \mu^k}{\partial n} = ik\phi^k \cdot \boldsymbol{n} - \dfrac{\boldsymbol{e}_\xi \times \phi_\eta^k + \phi_\xi^k \times \boldsymbol{e}_\eta}{||\boldsymbol{e}_\xi \times \boldsymbol{e}_\eta||} \cdot \boldsymbol{i} & \text{on } S_B \\ \Delta \dfrac{\partial \mu^k}{\partial n} = 0 & \text{on } S_W \end{cases} \tag{15}$$

where Ω is the flow domain, and its boundaries are the closed surface of the body S_B, and the open surface of the wake S_W.

We can define a sub-differentiation process in which we seek the derivative of Q_{hk} with eqs.(15) as disciplinary equations, and the potential μ as state variable. Although not exploited in this work, the methods and procedures developed here can be used for shape and structural optimization, for example using the free-form deformation (FFD) technique for the outer mold line parametrization, and the structural element thickness as structural design variables. Therefore, the number of design variables is potentially significantly greater than the number of elements of the GAF matrix, making the adjoint method the preferred approach for the computation of the GAF derivative. Now, we focus on the computation of the partial sub-derivative of the function of interest, $Q_{hk}(\mu, \boldsymbol{t})$, and the disciplinary equations, eqs.(15), which will be concisely referred as $R(\mu, \boldsymbol{t}) = 0$.

Following the so-called discrete adjoint approach, we first discretize $Q_{hk}(\mu, \boldsymbol{t})$ expression and eqs.(15), then we differetiate. After the discretization, the continuous state variable, the potential $\mu(\xi, \eta)$, is replaced by a vector of state variables, $\boldsymbol{\mu} = [\mu_1, \mu_2, \ldots, \mu_{N_p}]^T$, representing the potential on each panel.

Dividing the body surface in N_p panels, the expression of one element of the aerodynamic matrix, Q_{hk} becomes

$$Q_{hk}(\boldsymbol{t}, \boldsymbol{\mu}^k) = \sum_{i=1}^{N_p} \phi_i^h(\boldsymbol{t}) \cdot \boldsymbol{n}_i(\boldsymbol{t}) C_p^i(\boldsymbol{t}, \boldsymbol{\mu}^k) A_i(\boldsymbol{t}) \tag{16}$$

where C_p^i is the pressure coefficient on the i-th panel

$$C_p^i(\boldsymbol{t}, \boldsymbol{\mu}^k) = -2\left(ik/l\mu_i^k + \left(d_\xi^i(\boldsymbol{t}, \boldsymbol{\mu}^k)\boldsymbol{l}_i(\boldsymbol{t}) + d_\eta^i(\boldsymbol{t}, \boldsymbol{\mu}^k)\boldsymbol{m}_i(\boldsymbol{t}) + \sigma_i(\boldsymbol{t})\boldsymbol{n}_i(\boldsymbol{t})\right) \cdot \boldsymbol{i}\right) \tag{17}$$

The function d_ξ^i and d_η^i represents the surface derivative of the potential in the two tangential directions on the i-th panel. To compute this derivative, we use a finite difference method with a variable stencil; when possible the second order central schema is used otherwise the right or left second order, and, in the worst case, a first order schema. For example, assuming that for the i-th panel all the surrounding panels in the ξ direction are available, and that the panel numbering direction coincides with the xi direction, then $d_\xi^i(\boldsymbol{t}, \boldsymbol{\mu}^k) = a_i(\boldsymbol{t})\mu_{i-1}^k + b_i(\boldsymbol{t})\mu_{i+1}^k$, where $a_i(\boldsymbol{t})$ and $b_i(\boldsymbol{t})$ are the finite difference schema coefficients depending on the grid. The disciplinary equations, eq.(15), are reduced to the following linear system.

$$R(\boldsymbol{t}, \boldsymbol{\mu}) = \boldsymbol{AIC}_d(\boldsymbol{t})\boldsymbol{\mu}^k - \boldsymbol{AIC}_s(\boldsymbol{t})\boldsymbol{\sigma}^k(\boldsymbol{t}) = 0 \tag{18}$$

where $\sigma_i^k(\boldsymbol{t})$ represents the boundary condition on the i-th panel for the k-th shape deformation[4].

$$\sigma_i^k(\boldsymbol{t}) = ik\phi_i^k(\boldsymbol{t}) \cdot \boldsymbol{n}_i(\boldsymbol{t}) - \frac{\boldsymbol{e}_\xi^i(\boldsymbol{t}) \times \phi_{i,\eta}^k(\boldsymbol{t}) + \phi_{i,\xi}^k(\boldsymbol{t}) \times \boldsymbol{e}_\eta^i(\boldsymbol{t})}{||\boldsymbol{e}_\xi^i(\boldsymbol{t}) \times \boldsymbol{e}_\eta^i(\boldsymbol{t})||} \cdot \boldsymbol{i} \tag{19}$$

The kutta condition on the wake is implemented directly in the definition of $\boldsymbol{AIC}_d$. Next, we compute the derivative of the generalized aerodynamic forces matrix element $Q(\boldsymbol{t}, \boldsymbol{\mu})$ and the disciplinary equation $R(\boldsymbol{t}, \boldsymbol{\mu})$ with respect to the design variable t and the potential of the

[4]In eq.(19) the k indicate the shape deformation when is used as index, and the reduced frequency when multiply the imaginary unit i.

j-th panel, μ_j (the index h and k representing the shape functions are dropped for the sake of simplicity). It is important to note that the imaginary component is introduced only by the body boundary condition $\boldsymbol{\sigma}$ and the wake boundary condition, in $\boldsymbol{AIC}_d$. Therefore for all the other variables we can use the complex step method (CS) to compute the partial derivative with respect to the design variables.

Partial derivative of the GAF matrix with respect to the design variables.

$$\begin{aligned}\frac{\partial Q}{\partial t} &= \frac{\partial}{\partial t}\sum_{i=1}^{N_p}\phi_i(\boldsymbol{t})\cdot\boldsymbol{n}_i(\boldsymbol{t})C_p^i(\boldsymbol{t},\boldsymbol{\mu})A_i(\boldsymbol{t}) \\ &= \sum_{i=1}^{N_p}\left(\frac{\partial\phi_i}{\partial t}\cdot\boldsymbol{n}_i C_p^i A_i + \phi_i\cdot\frac{\partial\boldsymbol{n}_i}{\partial t}C_p^i A_i + \phi_i\cdot\boldsymbol{n}_i\frac{\partial C_p^i}{\partial t}A_i + \phi_i\cdot\boldsymbol{n}_i C_p^i\frac{\partial A_i}{\partial t}\right)\end{aligned}$$

where

- $\frac{\partial\phi_i}{\partial t}$ is the derivative of the structural eigenvector calculated by the method described in subsection 3.2.
- $\frac{\partial\boldsymbol{n}_i}{\partial t}, \frac{\partial A_i}{\partial t}$ are obtained with the complex step method.
- $\frac{\partial C_p^i}{\partial t} = -2\left(d_\xi^i\frac{\partial\boldsymbol{l}_i}{\partial t} + d_\eta^i\frac{\partial\boldsymbol{m}_i}{\partial t} + \sigma_i\frac{\partial\boldsymbol{n}_i}{\partial t} + \frac{\partial d_\xi^i}{\partial t}\boldsymbol{l}_i + \frac{\partial d_\eta^i}{\partial t}\boldsymbol{m}_i + \frac{\partial\sigma_i}{\partial t}\boldsymbol{n}_i\right)\cdot\boldsymbol{i}$, where the derivative of the panel unit vectors, $\boldsymbol{l}$, $\boldsymbol{m}$ and $\boldsymbol{n}$, can be obtained with the complex step method. The derivative of the normal-wash, $\frac{\partial\sigma_i}{\partial t}$, appears also in the derivative of R with respect to the design variable t, and is extensively analyzed in the following subsection.
- $\frac{\partial d_\xi^i}{\partial t} = \frac{\partial a_i}{\partial t}\mu_{i-1} + \frac{\partial b_i}{\partial t}(\boldsymbol{t})\mu_{i+1}$, since $a_i(\boldsymbol{t})$ and $b_i(\boldsymbol{t})$ are real variables, the complex step method is used to compute the needed derivatives.
- $\frac{\partial d_\eta^i}{\partial t} = \frac{\partial c_i}{\partial t}\mu_{i-1} + \frac{\partial d_i}{\partial t}(\boldsymbol{t})\mu_{i+1}$, as above.

Derivative of the GAF matrix with respect to the state variables.

$$\frac{\partial Q}{\partial\mu_j} = \frac{\partial}{\partial\mu_i}\sum_{i=1}^{N_p}\phi_i(\boldsymbol{t})\cdot\boldsymbol{n}_i(\boldsymbol{t})C_p^i(\boldsymbol{t},\boldsymbol{\mu})A_i(\boldsymbol{t}) = \sum_{i=1}^{N_p}\phi_i\cdot\boldsymbol{n}_i\frac{\partial C_p^i}{\partial\mu_i}A_i$$

where

- $\frac{\partial C_p^i}{\partial\mu_j} = -2\left[\frac{ik}{l}\delta_{ij} + \left(\frac{\partial d_\xi^i}{\partial\mu_j}\boldsymbol{l}_i + \frac{\partial d_\eta^i}{\partial\mu_j}\boldsymbol{m}_i\right)\cdot\boldsymbol{i}\right]$, where δ_{ij} is the Kronecker's delta.
- $\frac{\partial d_\xi^i}{\partial\mu_j} = a_i(\boldsymbol{t})\delta_{i-1,j} + b_i(\boldsymbol{t})\delta_{i+1,j}$
- $\frac{\partial d_\eta^i}{\partial\mu_j} = c_i(\boldsymbol{t})\delta_{i-1,j} + d_i(\boldsymbol{t})\delta_{i+1,j}$

Derivative of the disciplinary equations with respect to the design variables.

$$\frac{\partial R}{\partial t} = \frac{\partial}{\partial t}\left(\boldsymbol{AIC}_d(\boldsymbol{t})\boldsymbol{\mu} - \boldsymbol{AIC}_s(\boldsymbol{t})\boldsymbol{\sigma}(\boldsymbol{t})\right) = \frac{\partial\boldsymbol{AIC}_d}{\partial t}\boldsymbol{\mu} - \frac{\partial\boldsymbol{AIC}_s}{\partial t}\boldsymbol{\sigma} - \boldsymbol{AIC}_s\frac{\partial\boldsymbol{\sigma}}{\partial t}$$

where

$\frac{\partial \boldsymbol{AIC}_d}{\partial t} = \frac{\partial \boldsymbol{C}^s}{\partial t} + \frac{\partial \boldsymbol{W}^u}{\partial t}$, where $\boldsymbol{C}^s$ is matrix of the doublet-like body influence coefficients for the zero-frequency aerodynamics case, and $\boldsymbol{W}^u$ is the matrix of the doublet-like wake influence coefficients matrix containing the unsteady wake boundary condition.

$\frac{\partial C^s_{ij}}{\partial t}$ is obtained with the complex step method, since in the zero-frequency case there are only real terms.

$$\frac{\partial W^u_{ij}}{\partial t} = \begin{cases} 0 & \text{if panel } j \notin \text{TE} \\ \sum_{w=1}^{N_w} \left(\frac{\partial W^s_{iw}}{\partial t} e^{-ik/l\Delta_{w,TE}} - \frac{ik}{l} W^s_{iw} \frac{\partial \Delta_{w,TE}}{\partial t} e^{-ik/l\Delta_{w,TE}} \right) & \text{if panel } j \in \text{TE} \end{cases},$$

where $\boldsymbol{W}^s$ is the doublet-like body influence coefficients for the zero-frequency aerodynamics case, $\Delta_{w,TE}$ is the distance along the wake among the w-th wake panel and the associated trailing edge (TE) body panel, and N_w is the number of wake panel in stream-wise direction.

$\frac{\partial W^s_{iw}}{\partial t}, \frac{\partial \boldsymbol{AIC}_s}{\partial t}$ are computed with the complex step method, since in the zero-frequency case there are only real terms.

$\frac{\partial \Delta_{w,TE}}{\partial t}$ depends exclusively on the wake geometry, hence it is different from zero only for design variables that modify the trailing edge shape. It these case the complex step method is used.

$\frac{\partial \sigma_i}{\partial t} = \frac{\partial F_i}{\partial t} - \frac{\partial G_i}{\partial t}$, where $F_i(\boldsymbol{t})$ and $G_i(\boldsymbol{t})$ represent the imaginary and real part respectively of the body boundary condition on the i-th panel.

$\frac{\partial F_i}{\partial t} = ik \frac{\partial \boldsymbol{n}_i}{\partial t} \cdot \phi_i + ik \boldsymbol{n}_i \cdot \frac{\partial \phi_i}{\partial t}$, where both $\frac{\partial \boldsymbol{n}_i}{\partial t}$ and $\frac{\partial \phi_i}{\partial t}$ have been already obtained.

$\frac{\partial G_i}{\partial t} = g\left(\frac{\partial \boldsymbol{e}^i_\xi}{\partial t}, \frac{\partial \boldsymbol{e}^i_\eta}{\partial t}, \frac{\partial \phi_{i,\xi}}{\partial t}, \frac{\partial \phi_{i,\eta}}{\partial t} \right)$. This is the most demanding terms and highly depends on the surface parametrization. In particular, $(\boldsymbol{e}^i_\xi, \boldsymbol{e}^i_\eta)$ are the surface tangential vectors of the i-th panel, and $\phi_{i,\xi}$, $\phi_{i,\eta}$ the surface derivatives of the deformation shape function calculated on the i-th panel. Since $(\boldsymbol{e}^i_\xi, \boldsymbol{e}^i_\eta)$ are real variables we use the complex step method to compute their derivative. Instead for the mixed derivative, $\phi_{i,\xi t}$, $\phi_{i,\eta t}$ we use the following procedure:

1. compute the derivative of the modal shapes with respect to the design variables, ϕ_t, with the method described in subsection 3.2;
2. perform the surface differentiation of ϕ_t, obtaining $\phi_{t,\xi}$ and $\phi_{t,\eta}$;
3. Then, assuming ϕ to be a continuous function and with a continuous derivative with respect to both design variables and surface coordinates, the Schwarz's theorem apply: $\phi_{\xi t} = \phi_{t\xi}$, and $\phi_{\eta t} = \phi_{t\eta}$

Derivative of the disciplinary equations with respect to the state variables.

$$\frac{\partial R}{\partial \mu_j} = \frac{\partial}{\partial \mu_j} \left(\boldsymbol{AIC}_d(\boldsymbol{t})\boldsymbol{\mu} - \boldsymbol{AIC}_s(\boldsymbol{t})\boldsymbol{\sigma}(\boldsymbol{t}) \right) = [\boldsymbol{AIC}_d]_j$$

that is the j-th column of the matrix $\boldsymbol{AIC}_d$.

3.2 Derivative of Modal Shapes

The derivative of the stiffness, damping and mass matrices are assembled starting from the derivative of the single finite element, and the latter are obtained analytically given the low complexity of our structural model. Focus of this subsection is the differentiation of the structural modal shapes, $\boldsymbol{\phi}$, with respect to the design variable, t.

The structural modal analysis equation is[5]

$$(\boldsymbol{K} - \lambda \boldsymbol{M})\boldsymbol{\phi} = 0 \tag{20}$$

where λ is the square of the natural frequency. Following the procedure proposed by Cardani and Mantegazza in [17], instead of solving eq. (20) as an eigenvalue problem, it is observed that only the direction of the eigenvector $\boldsymbol{\phi}$ is defined, not its module. Therefore, in order to close the system a normalization equation is added and the obtained system, eq. (3.2), can be solved as a standard non-linear system, for instance we use the Newton-Raphson method.

$$\begin{cases} (\boldsymbol{K} - \lambda \boldsymbol{M})\boldsymbol{\phi} = 0 \\ \boldsymbol{\phi}^T \boldsymbol{W} \boldsymbol{\phi} = 1 \end{cases}$$

Usually the matrix of weights, $\boldsymbol{W}$ is a combination of the structural matrices, we use $\boldsymbol{W} = \boldsymbol{M}$. Next we directly differentiate system (3.2) with respect to the design variables obtaining the derivative of the eigenvector and eigenvalue with respect to the design variables.

$$\begin{bmatrix} (\boldsymbol{K} - \lambda \boldsymbol{M}) & -\boldsymbol{M}\boldsymbol{\phi} \\ 2\boldsymbol{\phi}^T \boldsymbol{W} & 0 \end{bmatrix} \begin{Bmatrix} \frac{\partial \boldsymbol{\phi}}{\partial t} \\ \frac{\partial \lambda}{\partial t} \end{Bmatrix} = \begin{Bmatrix} -(\frac{\partial \boldsymbol{K}}{\partial t} - \lambda \frac{\partial \boldsymbol{M}}{\partial t})\boldsymbol{\phi} \\ 0 \end{Bmatrix} \tag{21}$$

In order to validate the procedure we carried out a comparison with complex step and finite difference methods. Figure 9 and 10 shows a good agreement between the implemented analytic procedure and the complex step method for the derivative of both eigenvalue and eigenvectors.

4 RESULTS

The Goland's wing is considered as a first test case for the flutter speed derivative procedure. This is a classical reference case for validation studies. Details of the model geometry and structure can be found in [38].
Obtained results show a good agreement with literature data. In particular, Goland's wing exhibits a typical flutter mechanism due to the coupling between the first bending and torsional mode (represented in figure 11), the natural frequency of these two modes are found at 7.88 Hz and 13.87 Hz respectively. At sea level ($\rho = 1.225$ kg/m^3), flutter is found at $U_F = 146.63$ m/s and $f_F = 10.36$ Hz (figure 12 and 13) that is in good agreement with literature results.

After the flutter analysis, we deploy the differentiation procedure. Figure 14 shows the comparison between finite difference and the implemented procedure on the derivative of flutter speed with respect to the span, whereas figure 15 concerns the derivative with respect to the sweep angle.
As expected, the derivative of flutter speed with respect to the span is negative, and significantly higher in absolute value than the derivative with respect to the sweep. The relative error, ϵ, between our methods and the finite difference derivatives presents the expected behavior. For high value of the step size the error decreases linearly, then after reaching the minimum point the error grows again for lower values of the step size.
The minimum found value of the relative error for the flutter speed derivative with respect to span and sweep is 9×10^{-4} and 2.5^{-2} respectively. Due to the well know numerical problem of the finite difference approach no better agreement was expected. Although these results confirm the accuracy of the implemented procedure, a definite validation can be obtained only by comparison with complex step, and it will be carried out in the following work.

[5]For the sake of simplicity we do not consider the damping matrix, but the described procedure does apply also in this case.

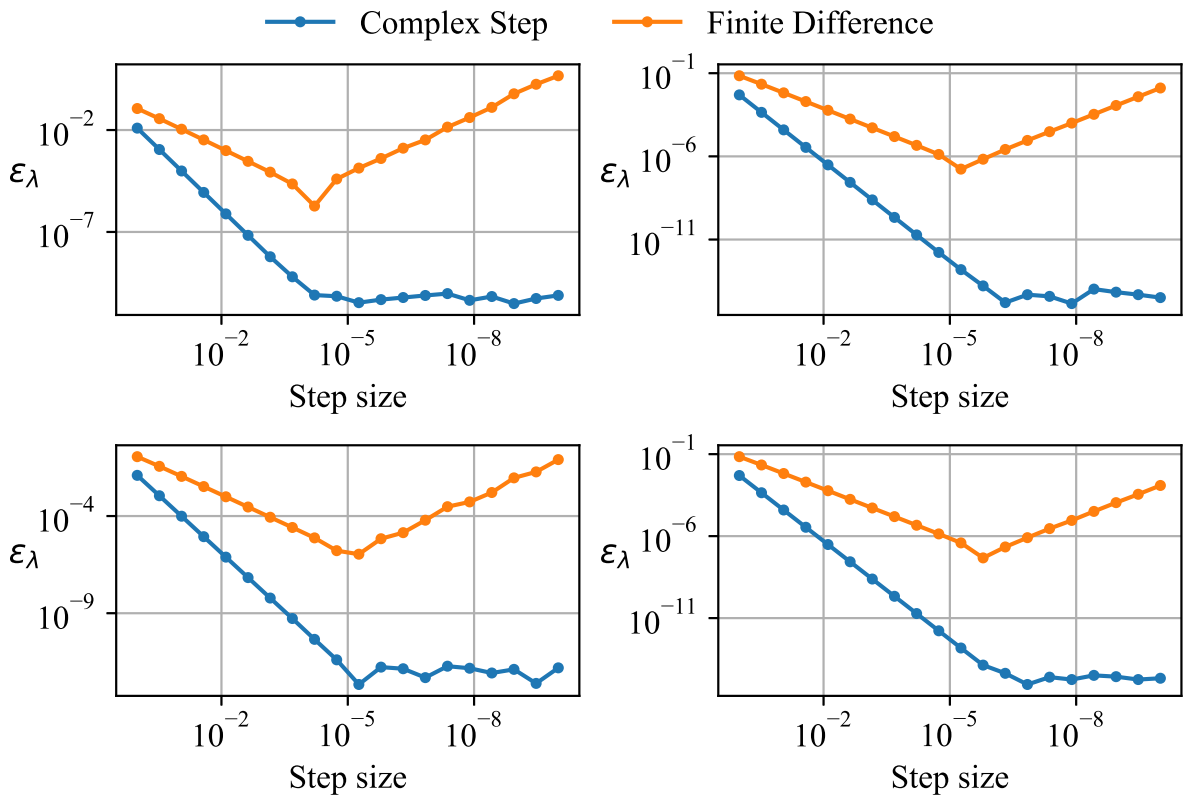

Figure 9: **Relative error on the span derivative of the first** 4 **structural eigenvalues for the Goland's wing.**

5 CONCLUSIONS

In this paper a procedure to compute the flutter speed derivative with respect to wing planform parameter is presented and implemented. This procedure is based on a 3D boundary element method, Morino's method for frequency domain aerodynamic analysis, and exploit the finite state aerodynamic modeling to represent the aerodynamic term in the aeroelastic equation.

Morino's method is able to consider arbitrary complex 3D body shapes increasing the fidelity of the unsteady aerodynamic analysis, and provides the necessary robustness for the deployment in a large scale MDO process.

The finite state aerodynamic modeling allows for the use of simple root locus method for the computation of the flutter point. In this way, the complex iterative procedure typical of *p-k* methods is avoided, and the accuracy of aeroelastic eigenvalues computation far from the flutter point is increased.
Moreover, by using the finite state finite state approach it is possible to define analytically the flutter speed derivative starting from the derivative of the structural and the aerodynamic terms. The derivative of the structural mass, stiffness and damping matrices are obtained analytically, whereas for the aerodynamic term, the GAF matrix, a discrete adjoint procedure is set up.

Since the goal here is to consider derivatives with respect to wing parameters, such as span or sweep angle, the derivative of structural modal shapes cannot be neglected as typically done for structural design variables, and, thus, they are analytically computed.
The partial derivative of the zero-frequency aerodynamic contribution to the GAF is computed with complex step, since this part of the computation involves only real value variables, and

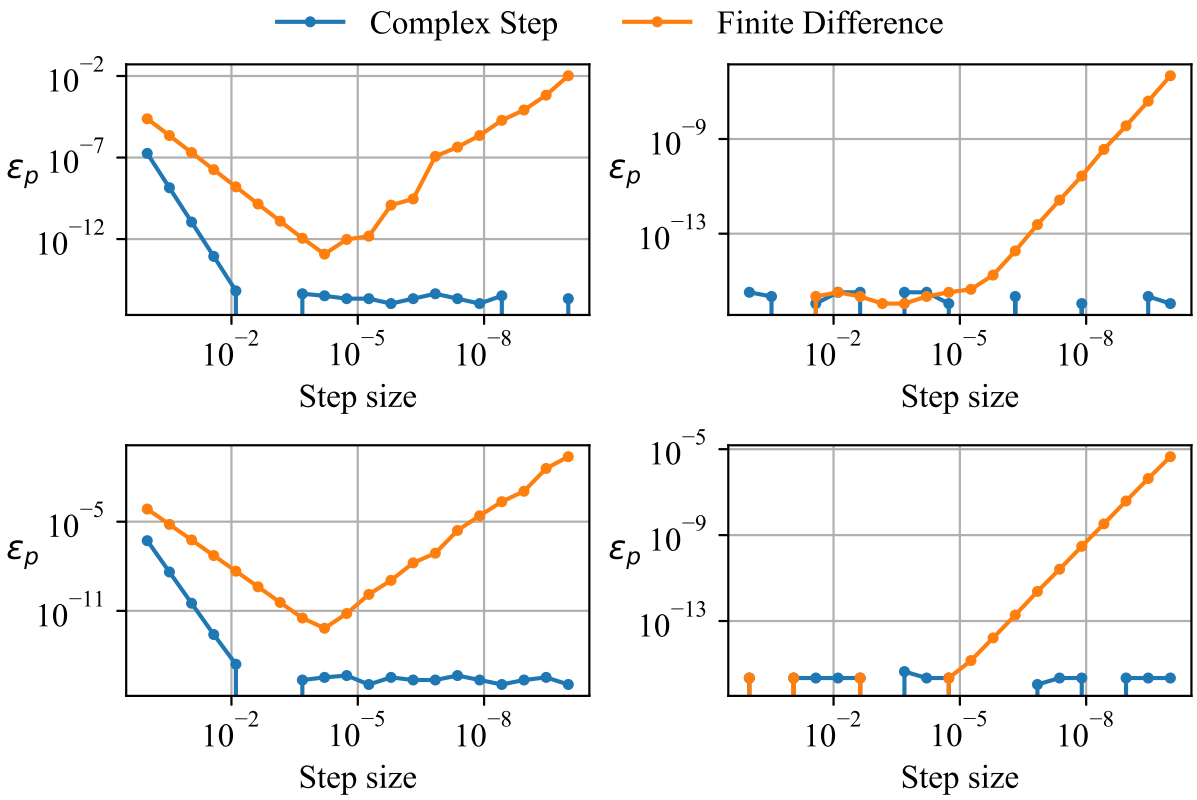

Figure 10: **Parallelism test of the span derivative of the first 4 structural eigenvectors for the Goland's wing.**

the number of function of interest are equal if not greater than the number of design variables. Starting from these terms the derivative of the unsteady complex variables are assembled analytically, and then the total derivative of GAF is computed with an adjoint approach. The entire procedure is here described in detailed.

Flutter analysis is validated with a classical aeroelastic benchmark: Goland's wing. Obtained results show a good agreement with literature. The same use case is used to carry out a validation on the analytic differentiation procedure. Flutter speed derivative with respect to span and sweep are compared with finite difference results showing a good agreement.

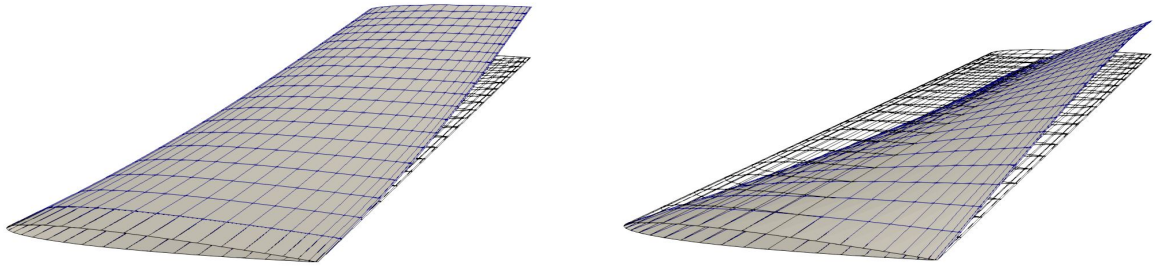

Figure 11: **Goland wing model first bending (left) and first torsional modal shape.**

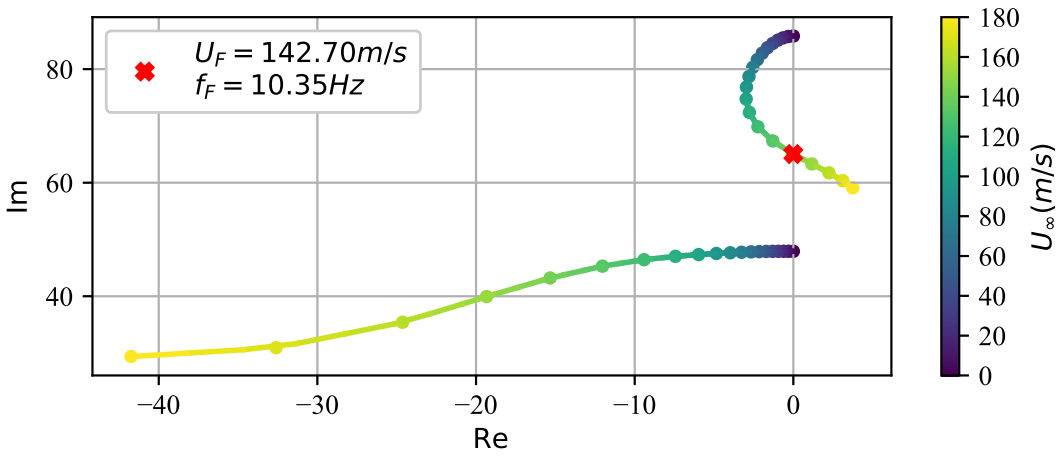

Figure 12: **Root locus of Goland's wing at sea level.**

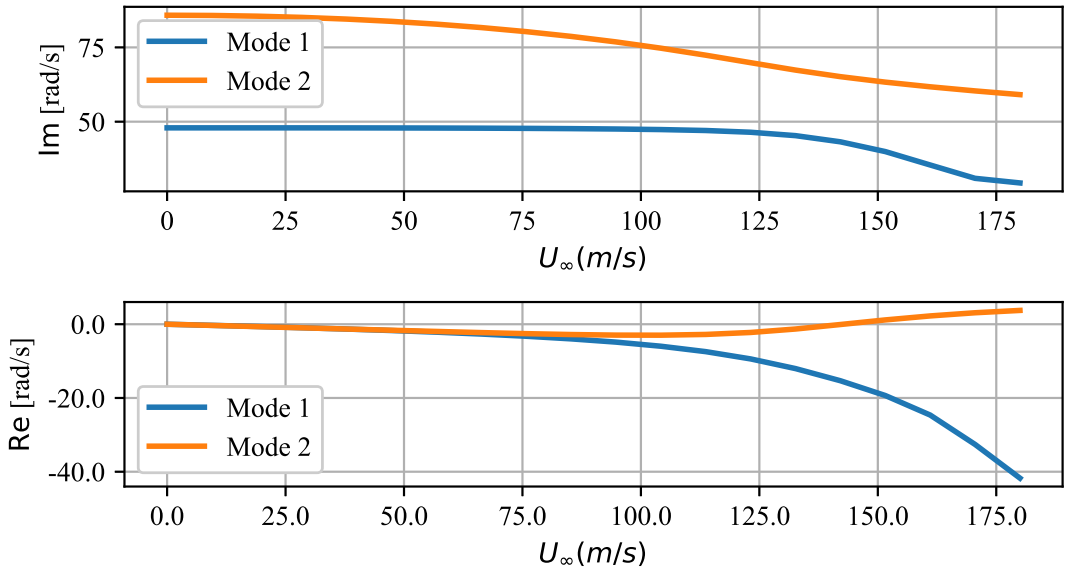

Figure 13: **The real and imaginary part of the aeroelastic eigenvalues of Goland's wing at sea level.**

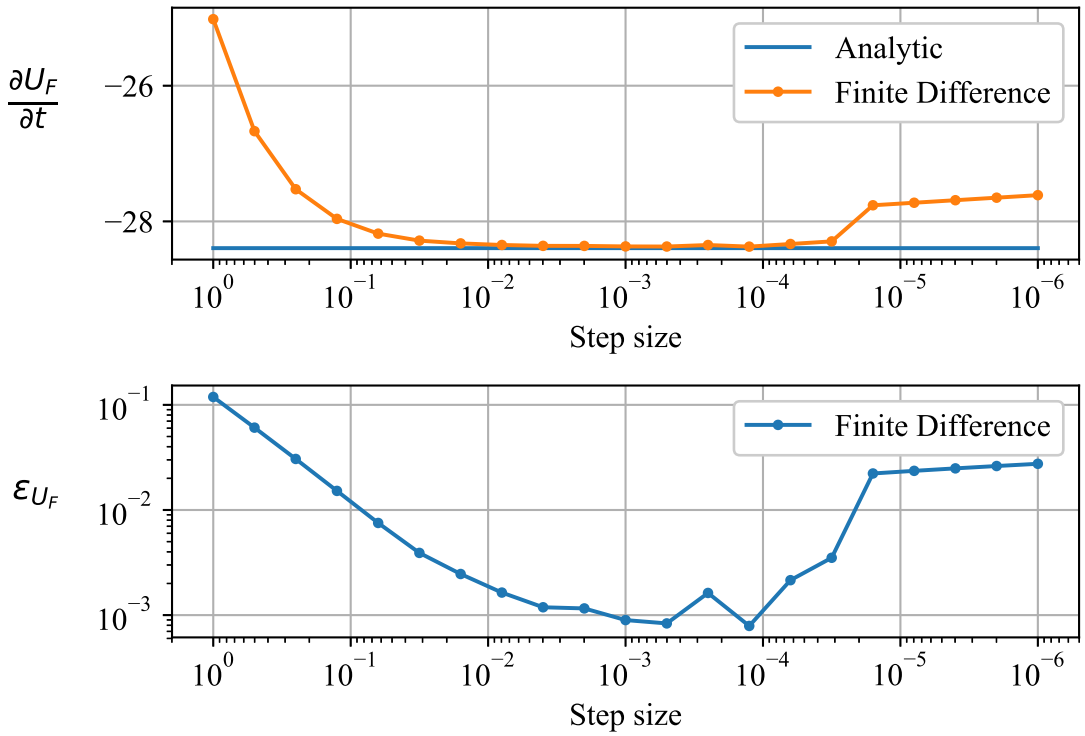

Figure 14: **Derivative of flutter speed with respect to span, $\frac{\partial U_F}{\partial t}$, for the Goland's wing. On the bottom the relative error, ε_{U_F}, between the implemented analytic procedure and finite difference.**

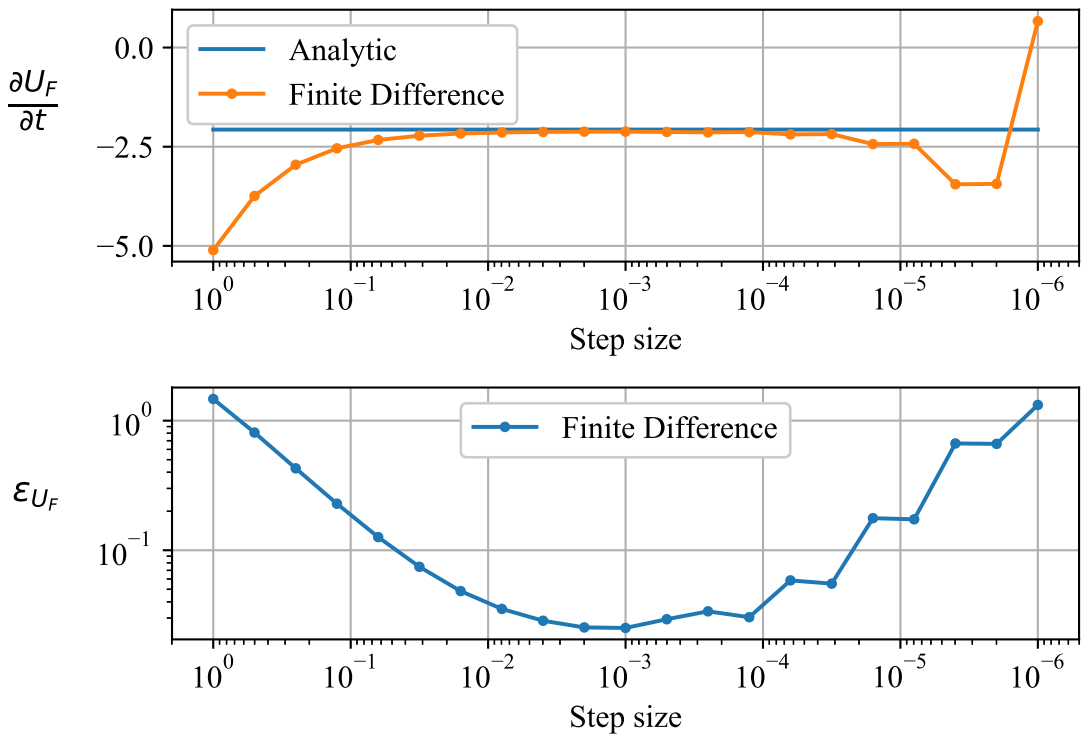

Figure 15: **Derivative of flutter speed with respect to sweep, $\frac{\partial U_F}{\partial t}$, for the Goland's wing. On the bottom the relative error, ε_{U_F}, between the implemented analytic procedure and finite difference.**

6 REFERENCES

[1] Henshaw, M. J. d. C., Badcock, K. J., Vio, G. A., et al. (2007). Non-linear aeroelastic prediction for aircraft applications. *Progress in Aerospace Sciences*, 43(4-6), 65–137. doi:10.1016/j.paerosci.2007.05.002.

[2] Livne, E. (1999). Integrated aeroservoelastic optimization: Status and direction. *Journal of Aircraft*, 36(1), 122–145. doi:10.2514/2.2419.

[3] Gu, X. (2017). *Application of CFD Based Aerodynamic Analysis and Optimization in a Multi-Fidelity Distributed Overall Aircraft Design System*. Ph.D. thesis, RWTH Aachen University.

[4] Kenway, G. K. W. and Martins, J. R. R. A. (2014). Multipoint high-fidelity aerostructural optimization of a transport aircraft configuration. *Journal of Aircraft*, 51(1), 144–160. doi:10.2514/1.c032150.

[5] Ciampa, P. D., Zill, T., and Nagel, B. (2012). Aeroelastic design and optimization of unconventional aircraft configurations in a distributed design environment. In *53rd AIAA/ASME/ASCE/AHS/ASC Structures, Structural Dynamics and Materials Conference*. American Institute of Aeronautics and Astronautics. doi:10.2514/6.2012-1925.

[6] Kapania, R. K., Jr., F. D. B., and Barthelemy, J.-F. M. (1991). Shape sensitivity analysis of flutter response of a laminated wing. *AIAA Journal*, 29(4), 611–612. doi:10.2514/3.59930.

[7] Issac, J., Kapania, R., and Barthelemy, J.-F. (1994). Sensitivity analysis of flutter response of a wing incorporating finite-span corrections. In *5th Symposium on Multidisciplinary Analysis and Optimization*. American Institute of Aeronautics and Astronautics. doi:10.2514/6.1994-4398.

[8] Yang, C., Yang, Y., and Wu, Z. (2012). Shape sensitivity analysis of flutter characteristics of a low aspect ratio supersonic wing using analytical method. *Science China Technological Sciences*, 55(12), 3370–3377. doi:10.1007/s11431-012-4933-3.

[9] Crema, L. B., Mastroddi, F., and Coppotelli, G. (2000). Aeroelastic sensitivity analyses for flutter speed and gust response. *Journal of Aircraft*, 37(1), 172–180. doi:10.2514/2.2577.

[10] Cavagna, L., Ricci, S., and Travaglini, L. (2011). NeoCASS: An integrated tool for structural sizing, aeroelastic analysis and MDO at conceptual design level. *Progress in Aerospace Sciences*, 47(8), 621–635. doi:10.1016/j.paerosci.2011.08.006.

[11] Stanford, B. K. and Dunning, P. D. (2015). Optimal topology of aircraft rib and spar structures under aeroelastic loads. *Journal of Aircraft*, 52(4), 1298–1311. doi:10.2514/1.c032913.

[12] van Zyl, L. H. (2001). Aeroelastic divergence and aerodynamic lag roots. *Journal of Aircraft*, 38(3), 586–588. doi:10.2514/2.2806.

[13] Jonsson, E., Kenway, G. K. W., Kennedy, G. J., et al. (2017). Development of flutter constraints for high-fidelity aerostructural optimization. In *35th AIAA Applied Aerodynamics Conference*. American Institute of Aeronautics and Astronautics. doi:10.2514/6.2017-4455.

[14] Jonsson, E., Mader, C. A., Kennedy, G., et al. (2019). Computational modeling of flutter constraint for high-fidelity aerostructural optimization. In *AIAA Scitech 2019 Forum*. American Institute of Aeronautics and Astronautics. doi:10.2514/6.2019-2354.

[15] Kennedy, G. J. and Martins, J. R. (2014). A parallel finite-element framework for large-scale gradient-based design optimization of high-performance structures. *Finite Elements in Analysis and Design*, 87, 56–73. doi:10.1016/j.finel.2014.04.011.

[16] Morino, L. (1974). A general theory of unsteady compressible potential aerodynamics. Tech. rep., NASA.

[17] Cardani, C. and Mantegazza, P. (1979). Calculation of eigenvalue and eigenvector derivatives for algebraic flutter and divergence eigenproblems. *AIAA Journal*, 17(4), 408–412. doi:10.2514/3.61140.

[18] https://www.cpacs.de/.

[19] https://rcenvironment.de/.

[20] Albano, E. and Rodden, W. P. (1969). A doublet-lattice method for calculating lift distributions on oscillating surfaces in subsonic flows. *AIAA Journal*, 7(2), 279–285. doi:10.2514/3.5086.

[21] MSC Software Corp (2012). *MSC Nastran 2012 Release Guide*.

[22] ZONA Technology (2008). *ZAERO Theoretical Manual*.

[23] Morino, L. (1973). Unsteady compressible potential flow around lifting bodies - general theory. In *11th Aerospace Sciences Meeting*. American Institute of Aeronautics and Astronautics. doi:10.2514/6.1973-196.

[24] Torrigiani, F. and Ciampa, P. D. (2018). Development of an unsteady aeroelastic module for a collaborative aircraft MDO. In *2018 Multidisciplinary Analysis and Optimization Conference*. American Institute of Aeronautics and Astronautics. doi:10.2514/6.2018-3879.

[25] Demasi, L. and Livne, E. (2009). Dynamic aeroelasticity of structurally nonlinear configurations using linear modally reduced aerodynamic generalized forces. *AIAA Journal*, 47(1), 70–90. doi:10.2514/1.34797.

[26] Morino, L., Mastroddi, F., Troia, R. D., et al. (1995). Matrix fraction approach for finite-state aerodynamic modeling. *AIAA Journal*, 33(4), 703–711. doi:10.2514/3.12381.

[27] Stanford, B. K. (2015). Role of unsteady aerodynamics during aeroelastic optimization. *AIAA Journal*, 53(12), 3826–3831. doi:10.2514/1.j054314.

[28] Karpel, M. (1982). Design for active flutter suppression and gust alleviation using state-space aeroelastic modeling. *Journal of Aircraft*, 19(3), 221–227. doi:10.2514/3.57379.

[29] Bombardieri, R., Auricchio, F., and Cavallaro, R. (2017). Unified longitudinal flight-dynamic and aeroelastic analysis of a prandtlplane configuration. In *Proceedings of the 6th CEAS Conference*. Bucharest.

[30] Raveh, D., Levy, Y., and Karpel, M. (2000). Aircraft aeroelastic analysis and design using CFD-based unsteady loads. In *41st Structures, Structural Dynamics, and Materials Conference and Exhibit*. American Institute of Aeronautics and Astronautics. doi: 10.2514/6.2000-1325.

[31] Bombardieri, R., Cavallaro, R., de Teresa, J. L. S., et al. (2019). Nonlinear aeroelasticity: a CFD-based adaptive methodology for flutter prediction. In *AIAA Scitech 2019 Forum*. American Institute of Aeronautics and Astronautics. doi:10.2514/6.2019-1866.

[32] Roger, K. L. (1977). Airplane math modelling methods for active control design. Tech. rep., AGARD.

[33] Gennaretti, M., Gori, R., Serafini, J., et al. (2015). Rotor dynamic wake inflow modelling in state-space format. In *33rd AIAA Applied Aerodynamics Conference*. American Institute of Aeronautics and Astronautics. doi:10.2514/6.2015-2885.

[34] van Zyl, L. H. (1993). Use of eigenvectors in the solution of the flutter equation. *Journal of Aircraft*, 30(4), 553–554. doi:10.2514/3.46380.

[35] Beckert, A. and Wendland, H. (2001). Multivariate interpolation for fluid-structure-interaction problems using radial basis functions. *Aerospace Science and Technology*, 5(2), 125–134. doi:10.1016/s1270-9638(00)01087-7.

[36] Rendall, T. C. S. and Allen, C. B. (2008). Unified fluid–structure interpolation and mesh motion using radial basis functions. *International Journal for Numerical Methods in Engineering*, 74(10), 1519–1559. doi:10.1002/nme.2219.

[37] Walther, J.-N., Gastaldi, A.-A., Mairel, R., et al. (2018). Integration aspects of the collaborative aero-structural design of an unmanned aerial vehicle. In *In Proceedings of DLRK*. Friedrichshafen.

[38] Goland, M. (1945). The flutter of a uniform cantilever wing. *Journal of Applied Mechanics*, 12(4), A197–A208.